Enhanced thermoelectric performance of $CuGaTe_2$ by Gd-doping and Te incorporation

Jian Zhang, Xiaoying Qin*, Di Li, Chunjun Song, Xiaoguang Zhu, Yongfei Liu, Hongxing Xin, Li Chen and Tianhua Zou

Key Laboratory of Materials Physics, Institute of Solid State Physics, Chinese Academy of Sciences, 230031 Hefei, P. R. China.

**Corresponding author:Tel: +86-551-65592750, Fax: +86-551-65591434,*

E-mail: xyqin@issp.ac.cn

Gd-doped compounds $CuGa_{1-x}Gd_xTe_2$ ($0 \le x \le 0.02$) incorporated with tellurium nanoparticles are synthesized by fusion method. Their thermoelectric properties are investigated in the temperature range of 300-800K. The results indicate that the synergistic effect of Gd-doping and Te incorporation remarkably enhances the thermoelectric performance of $CuGaTe_2$. Specially, the thermal conductivity κ of the specimen $CuGa_{0.98}Gd_{0.02}Te_2$/*0.7vol.%*Te reduces to 0.45 $Wm^{-1}K^{-1}$ at 684K, which is ~74% smaller than that of pure $CuGaTe_2$ (κ=1.76 $W \cdot m^{-1} \cdot K^{-1}$ at 684K) due to the incorporation of nanostructure Te. The thermoelectric figure of merit value (ZT) reaches 0.75 at 737K for the specimen $CuGa_{0.99}Gd_{0.01}Te_2$/0.7*vol.%*Te, which is ~115% larger than that of pure $CuGaTe_2$.

Keywords: A. Composite

B. Thermoelectric properties

C. Powder metallurgy

D. Microstructure

1. Introduction

In the last few decades, much attention has been focused on the field of thermoelectrics driven by the compelling need for more efficient and environmentally friendly energy conversion technologies [1-6]. However, the relatively low efficiencies of current thermoelectric (TE) device limit their large-scale commercialization [7-9]. The efficiency of TE device is determined by the TE figure of merit, defined by ZT ($ZT = S^2\sigma T/\kappa$), where S, σ, T, and κ are the electric conductivity, the Seebeck coefficient, the absolute temperature, and the thermal conductivity, respectively. A good TE material should possess a high power factor ($S^2\sigma$) and low thermal conductivity.

Many methods have been used to improve ZT of TE materials, among which element doping [10-17] aiming at optimization of carrier concentration and introduction of second phase [18-28] with nanosize designed to enhance Seebeck coefficient through an energy filtering effect and reduce the thermal conductivity by strengthened phonon scattering are effective way to enhance the TE performance. For example, Mn-substituted compound $Pb_{1-x}Mn_xTe$ [16] presented ZT=1.6 at 700K. Cui et al [17] synthesized the sample $Cu_{0.98}GaSb_{0.02}Te_2$, its ZT reached 1.07 at 721K. Li et al[19] obtained a high ZT value of 1.33 at 373K in $Bi_{0.3}Sb_{1.7}Te_3$ incorporated with only 0.4 vol % SiC nanoparticles. Zhai et al[21] reported a maximum ZT of 0.9 at 700K in In_4Se_3-based composite embedded with elemental indium. $CoSb_3$/grapheme [24] and CuInTe2/graphene[25] composites had the maximum ZT value of 0.61 (800K) and 0.40 (700K), respectively. And in the reference [26], through an energy filtering effect caused by carrier scattering at interface barriers and reduction in lattice thermal conductivity due to interface scattering, the ZT value reached 1.37 at 648K in the composite system β-Zn_4Sb_3 with 5vol.% of Cu_3SbSe_4. When a thermoelectric matrix is incorporated with a second phase, the interface scattering is expected to reduce the

thermal conductivity with slight effect on electrical conductivity[24]. Therefore, the nanocomposite approach is expected as the focus of future TE materials breakthroughs[29].

As a p-type semiconductor with E_g=1.2eV, $CuGaTe_2$ has chalcopyrite structure with the space group I-42d. $CuGaTe_2$ has been widely investigated as a promising candidate for thin film solar cells, photovoltaic devices, and so on [30-39]. Until recently, it was reported as a promising candidate for thermoelectric (TE) materials. Theerayuth Plirdpring et al [40] found that pure $CuGaTe_2$ has high ZT value at high temperature. However, few further optimizations [41-45] were realized for $CuGaTe_2$. In order to enhance the TE performance of $CuGaTe_2$, rare earth Gd atoms as dopant is introduced into the $CuGaTe_2$ matrix to substitute Ga sites, for the substitution of Gd for Ga atoms can produce lattice distortion and point defects, meanwhile, we introduce tellurium nanoparticles into the matrix as second phase. Through this approach we want to obtain smaller thermal conductivity κ due to effective scattering of acoustic phonons [47]. We have investigated the TE properties of the nanocomposites in the temperature range of 300-800K. The results indicated that our method effectively enhanced the thermoelectric performance of $CuGaTe_2$.

2. Experimental

Pure $CuGaTe_2$ and nanocomposites $CuGa_{1-x}Gd_xTe_2$/*f* Te with *x*= 0.005, 0.01, 0.02 and *f*=0.7vol% were prepared by a fusion method. Elemental copper (99.999wt.%), gadolinium (99.99wt.%), tellurium (99.999wt.%) powders and gallium chunk(99.99wt. %) were weighed accurately according to the desired composition, and sealed in an evacuated quartz tube, which were heat-treated in horizontal furnace at 1323 K for

24hours with the heating rate of 2 K/min. The obtained ingot is ground into powder. The powders about 2.5g are compacted by hot-pressing technique at a pressure of 300 MPa in a diameter of 15 mm tungsten carbide die in vacuum for 1 hours. The sintering temperature and heating rate are 623 K and 7 K/min, respectively. After a natural cooling process, bulk sample with dimensions of cylinder Φ15 mm × 2 mm in thickness can be obtained.

The product is characterized by X-raydiffraction (XRD) using Philips X'Pert PRO X-ray diffractometer equipped with graphite monochromatic Cu-Kα radiation (λ= 1.54056 Å). The operation voltage and current are kept at 40 kV and 400 mA, respectively. The accurate lattice parameters were determined from the *d* values of the XRD peaks using a standard least-squares refinement method with a Si standard for calibration. Microstructures were studied by using high resolution transmission electron microscopy (HTEM; JEOL JEM-2010) operating at a 200 kV accelerating voltage. The density*D* of hot-pressed bulk samples was determined by the Archimedes' method and found to be at least 97% of the theoretical density. The resistivity ρ and the Seebeck coefficient *S* were measured by using a commercially available instrument (ULVAC, ZEM-3) in He atmosphere. Thermal diffusivity (α) was measured by the laser flash method using a Netzsch LFA 457 instrument. The heat capacity C_p was obtained with a differential scanning calorimeter (DSC) (Perkin-Elmer, USA). Thermal conductivity κ was calculated based on the relationship $\kappa = \alpha \cdot C_p \cdot D$. The Hall coefficients were measured using the Van der Pauw technique under a magnetic field of 0.72 T.

3. Results and discussion

Fig.1(a) shows the powder XRD patterns of polycrystalline samples. It can be seen from Fig.1(a) with x=0 that the main diffraction peaks can be indexed to the phase of $CuGaTe_2$ (PDF#65-0244), belonging to the chalcopyrite structure, indicating that the specimens have the same crystallographic structure as that of $CuGaTe_2$(insert of Fig.1(a)). In comparison, three weak diffraction peaks (2θ=27.56°, 35.19° and 38.39° respectively) were observed for the samples with x=0.01 and x=0.02, which can be traced to the elemental Te (PDF#78-2312). Calculated from the XRD data, the lattice parameters *a* and *c* for $CuGaGdTe_2$ (x=0) and $CuGa_{1-x}Gd_xTe_2$/0.7vol% Te (x=0.005, 0.01, 0.02) are shown in table 1. *a* and *c* for pure $CuGaTe_2$ in this work are 6.021×10^{-10} m and 11.963×10^{-10} m, respectively, which are slightly different from the reported data (a=6.016×10^{-10}m and c = 11.942×10^{-10}m[40]). It can be seen that gadolinium doping causes the decrease in the lattice parameters *a* and *c*, which may be caused by the lattice distortion after Gd doping, as discussed below. The low-magnification bright-field TEM image for $CuGa_{0.99}Gd_{0.01}Te_2$/0.7vol.%Te (Fig. 1(b)) reveals that the particles with size of wide range from nanostructure (<~150nm) to micro-scale are observed. An amplified HRTEM image in the rectangle area in Fig. 1(b) is shown in Fig. 1(c), which indicates that the lattice spacing of about 3.85Å corresponds to (1 0 0) planes of hexagonal Te and the interplanar spacing of about 3.46 Å can be assigned to the (1 1 2) lattice plane of cubic $CuGaTe_2$. These results suggest that Te nanoparticles are embedded in $CuGaTe_2$ matrix, forming $CuGaTe_2$/0.7*vol.* %Te nano-composite.

The temperature dependence of electrical resistivity ρ for $CuGa_{1-x}Gd_xTe_2$/0.7*vol.*%Te ($0\leq x\leq0.02$) is shown in Fig. 2(a). ρ for pure$CuGaTe_2$ increases slightly with increasing

temperature until T~500K, and then decreases with further increasing the temperature ($d\rho/dT<0$), indicating that $CuGaTe_2$ is a thermal activated semiconducting behavior[48]. However, the metal-like behavior ($d\rho/dT>0$) in $\rho(T)$ curves is found for doped compound $CuGa_{1-x}Gd_xTe_2$ /0.7*vol.*%Te ($x>0$). In other words, a transition from semiconductor-like to metal-like behavior is occurred after Gd doping. In addition, the electrical resistivity for nano-composite $CuGa_{1-x}Gd_xTe_2$/0.7*vol.*%Te ($x>0$) is smaller than that of pure $CuGaTe_2$. The Hall coefficient, R_H, at room temperature (RT) is positive for $CuGaTe_2$, which indicates p-type or hole conduction in this system. Assuming parabolic bands and a single band conduction process at 300 K, we estimate the carrier concentration, p, from the formula: $p=1/eR_H$, where e is the carrier charge. The carrier concentrations p are 1.49×10^{19}, 3.87×10^{19} cm^{-3}, 2.17×10^{20} and 6.42×10^{20} cm^{-3} for x=0, 0.005, 0.01 and 0.02, respectively (Table 1). The holes concentration of pure $CuGaTe_2$ $p=1.49\times10^{19}$ cm^{-1} at room temperature, which is different from the reported data ($p=1.1\times10^{18}$ cm^{-3} [40] and $p=2.05\times10^{19}$ cm^{-3}[49]), which can lead to the difference in the electrical resistivity, for example, the report data [40] is nearly five times as the ρ value ($7.87\times10^{-5}\Omega\cdot m$) for pure $CuGaTe_2$ at room temperature. A small difference in the sample composition, such as the Te content, would lead to a distinct difference in holes concentration p and thermopower S values [40].

As we know, pure $CuGaTe_2$ is a *p*-type semiconductor [40]. However, one can find the transition from semiconducting to metal-like behavior after Gd substituting for Ga. The reason for the transition may be lie in that the holes concentration p for $CuGa_{1-x}Gd_xTe_2$/0.7*vol.*%Te increase after Gd substitution, which leads to the fact that Fermi

level E_F shift into (or near) valence band. As a result, a degenerated semiconductor has been formed. The value of holes concentration in room temperature increase rapidly from 1.49×10^{19} cm^{-3} to 3.87×10^{19} cm^{-3}, 2.17×10^{20} cm^{-3} with Gd doping content x increasing from 0 to 0.005 and 0.01, then holes concentration *p* increase slightly to 6.42×10^{20} cm^{-3} with Gd content x further increasing to 0.02. Since the radius of Gd^{3+} (0.94 Å) is larger than that of Ga^{3+} (0.62 Å), the substitution of Gd for Ga would produce lattice distortion and point defects e.g. vacancies of Cu and/or Ga, such as V_{Cu}' and V_{Ga}'''[46, 50]. And the lattice distortion has been verified by the measured lattice parameters as seen in table 1. It can be seen from table 1 that the value of c/a decrease from 1.999 to 1.987, 1.991, and then 1.982 with increasing Gd content x from 0 to 0.005, 0.01 and 0.02. This means that Gd doping in $CuGaTe_2$ will introduce acceptor levels into the gap and give rise to the increase in holes concentration. This is to say, Gd substitution for Ga acts as holes doping in this system, which can explain the obvious decrease of both electrical resistivity ρ and thermopower *S* after Gd doping at room temperature, as shown in Fig.2 (a) and (b). One can see from Fig.2 (b) that the sign of thernopower *S* for all specimens are positive, indicating that the majority of the carriers were holes. The values of *S* for doped compounds are smaller than that of pure $CuGaTe_2$ in almost whole investigated temperature range. One notices that for all samples values of *S* increase with increasing temperature in the investigated temperature range, which indicates that the transport behavior is dominated by intrinsic excitation at higher temperature , as demonstrated in table 1. Furthermore, the increased hole concentration

p also explains why *S* decreases with increasing Gd content, for *S* is inversely proportional to carrier concentration *p,* as expressed by Mott equation:

(1)

where σ is the electrical conductivity, q is the carrier charge, k_B is the Boltzmann constant, and E_f is the Fermi energy. One can see from equation (1) that *S* increases (or decrease) with decreasing (or increasing) *p*. Figure 2(b) shows that the room-temperature *S* decreases with increasing the Gd content, the value of *S* decreases from 42.0 to 24.1, 23.3 and 15.4 μVK^{-1}, accompanying with the increase in the hole concentration *p* from 1.49×10^{19} to 3.87×10^{19}, 21.7×10^{19} and 64.2×10^{19} cm^{-3}, respectively. One can notice that the value of *S* at room temperature is different from the report data [18, 40], which cause by the difference in the sample composition, as discussed above. Fig.2(c) shows the temperature dependence of power factor (PF) for $CuGa_{1-x}Gd_xTe_2$/0.7*vol.*%Te ($0\le x\le0.02$), we can see that the power factor for the pure $CuGaTe_2$ reached $0.85\times10^{-3}W\cdot m^{-1}\cdot K^{-2}$ at 763K, slightly larger than the report data ($\sim0.75\times10^{-3}W\cdot m^{-1}\cdot K^{-2}$ at 721K)[43] for the pure $CuGaTe_2$. It can be seen from Fig.2(c) that PF of the specimen of x=0.01 reached a maximum value of $0.58\times10^{-3}W\cdot m^{-1}\cdot K^{-2}$ at 737K. However, as the temperature further increasing, the power factors of Gd doped compounds $CuGa_{1-x}Gd_xTe_2$/0.7*vol.*%Te (x>0) present a drop due to the abrupt increase of the electrical resistivity.

Fig.3(a) shows the temperature dependence of thermal conductivity κ for $CuGa_{1-x}Gd_xTe_2$ /0.7*vol.*%Te ($0\le x\le0.02$). The value of κ decrease rapidly with increasing

temperature, indicating that phonon conductivity dominated κ for all the samples[48]. The κ values for the composite samples are smaller than that of pure $CuGaTe_2$ sample due to the incorporation of nano Te. Specially, the thermal conductivity of the specimen $CuGa_{0.98}Gd_{0.02}Te_2$/*0.7vol.%*Te decrease to 0.45 $Wm^{-1}K^{-1}$ at 684K, ~74% smaller than that of pure $CuGaTe_2$ (κ=1.76 $W\cdot m^{-1}\cdot K^{-1}$ at 684K), which ascribe to the remarkable decrease in lattice thermal conductivity κ_L. The total thermal conductivity κ can be expressed by the sum of lattice component (κ_l) and hole component (κ_h) as $\kappa=\kappa_l+\kappa_h$. The κ_h values can be estimated from Wiedemann-Franz's law as $\kappa_h=LT/\rho$ (here L is the Lorentz number, $L=1.5\times10^{-8}V^2K^{-2}$ [40] for $CuGa_{1-x}Gd_xTe_2$/0.7*vol.*%Te (0≤x≤0.02), as seen in figure 3(b). Consequently, κ_L can be obtained from κ and κ_h, as shown in Fig.3(c). It can be seen by comparing Fig.3(a) with Fig.3(c) that the values and temperature dependences of lattice conductivity κ_L are similar to those of the total thermal conductivity κ. These results indicate that thermal conductivity of $CuGa_{1-x}Gd_xTe_2$/0.7*vol.*%Te (0≤x≤0.02) come mainly from their lattice conductivity. Obviously, we can see from figure 3(c) that lattice conductivity κ_L of Gd-doped samples present an abruptly drop at ~600K, which cause by the melting of nano tellurium particles (the melting point can become lower when the particles become smaller[52]).

The temperature dependence of ZT values for $CuGa_{1-x}Gd_xTe_2$/0.7*vol.*%Te (0≤x≤0.02) are shown in figure 3(d). One can see that the ZT values of all samples increased with increasing temperature in almost whole temperature range. ZT of the sample for x=0.01 have a maximum value, reaching 0.75 at 737K, which is ~115% larger than that of pure $CuGaTe_2$ at the same temperature (ZT=0.34 at 737K).

4. Conclusions

In summary, polycrystal samples $CuGa_{1-x}Gd_xTe_2$ ($0 \le x \le 0.02$) incorporated with nanostructured Te (0.7*vol.*%) were prepared by fusion method. The thermoelectric properties were investigated in 300-800K. The synergistic effect of Gd-doping and Te incorporation is proved to an effective method to tuning the carrier concentration and lowering the value of thermal conductivity, thereby enhancing the thermoelectric properties of $CuGaTe_2$. The sample $CuGa_{0.99}Gd_{0.01}Te_2$/0.7*vol.*% has the largest ZT value, reaching 0.75 at 737 K, which is ~115% larger than that of pure $CuGaTe_2$ at the same temperature. And the maximum 0.75 is 25% larger than the report data (ZT~0.6 at 737K) [40]. All the results indicated that $CuGa_{0.99}Gd_{0.01}Te_2$/0.7*vol.*% is a promising candidate as a thermoelectric material in the middle temperature range.

Acknowledgement

Financial support from Anhui Provincial Natural Science Foundation (No. 1408085QB45) and national natural science foundation of China (Nos. 11174292, 11374306, and 10904144 is gratefully acknowledged.

References:

[1] P. Puneet, R. Podila, S. Zhu, M.J. Skove, T.M. Tritt, J. He, A.M. Rao, Adv Mater, 25 (2013) 1033-1037.
[2] Y.X. Chen, B.L. Du, Y. Saiga, K. Kajisa, T. Takabatake, J Phys D Appl Phys, 46 (2013).
[3] D. Wu, A.S. Petersen, S.J. Poon, Aip Adv, 3 (2013) 9.
[4] X. Ye, Y. Junyou, L. Gen, L. Ming, F. Liangwei, L. Yubo, L. Weixin, P. Jiangying, Intermetallics, 50 (2014) 20-27.
[5] R. Chetty, D.S.P. Kumar, M. Falmbigl, P. Rogl, S.W. You, I.-H. Kim, R.C. Mallik, Intermetallics, 54 (2014) 1-6.
[6] R. Carlini, D. Marre, I. Pallecchi, R. Ricciardi, G. Zanicchi, Intermetallics, 45 (2014) 60-64.
[7] F.J. Fan, Y.X. Wang, X.J. Liu, L. Wu, S.H. Yu, Adv Mater, 24 (2012) 6158-6163.
[8] D. Li, X.Y. Qin, Y.F. Liu, C.J. Song, L. Wang, J. Zhang, H.X. Xin, G.L. Guo, T.H. Zou, G.L. Sun, B.J. Ren, X.G. Zhu, RSC Advances, 4 (2014) 8638-8644.
[9] D. Li, R. Li, X.-Y. Qin, C.-J. Song, H.-X. Xin, L. Wang, J. Zhang, G.-l. Guo, T.-H. Zou, Y.-F. Liu, X.-G. Zhu, Dalton Transactions, 43 (2014) 1888-1896.
[10] J. Zhang, X.Y. Qin, D. Li, H.X. Xin, C.J. Song, L.L. Li, Z.M. Wang, G.L. Guo, L. Wang, Journal of Alloys and Compounds, 586 (2014) 285-288.
[11] D. Li, R. Li, X.Y. Qin, J. Zhang, C.J. Song, L. Wang, H.X. Xin, Crystengcomm, 15 (2013) 7166-7170.
[12] W.J. Xie, S. Populoh, K. Galazka, X.X. Xiao, L. Sagarna, Y.F. Liu, M. Trottmann, J. He, A. Weidenkaff, J Appl Phys, 115 (2014).

[13] C. Wang, Y.X. Wang, G.B. Zhang, C.X. Peng, G. Yang, Phys Chem Chem Phys, 16 (2014) 3771-3776.
[14] N. Prasoetsopha, S. Pinitsoontorn, T. Kamwanna, V. Amornkitbamrung, K. Kurosaki, Y. Ohishi, H. Muta, S. Yamanaka, J Alloy Compd, 588 (2014) 199-205.
[15] A. Mehdizadeh Dehkordi, S. Bhattacharya, T. Darroudi, J.W. Graff, U. Schwingenschlögl, H.N. Alshareef, T.M. Tritt, Chem Mater, (2014) dx.doi.org/10.1021/cm4040853.
[16] Y.Z. Pei, H. Wang, Z.M. Gibbs, A.D. LaLonde, G.J. Snyder, Npg Asia Mater, 4 (2012).
[17] J. Cui, Y. Li, Z. Du, Q. Meng, H. Zhou, J Mater Chem A, 1 (2013) 677-683.
[18] J. Zhang, X. Qin, D. Li, H. Xin, C. Song, L. Li, X. Zhu, Z. Wang, G. Guo, L. Wang, Journal of Materials Chemistry A, 2 (2014) 2891-2895.
[19] J. Li, Q. Tan, J.-F. Li, D.-W. Liu, F. Li, Z.-Y. Li, M. Zou, K. Wang, Adv Funct Mater, 23 (2013) 4317-4323.
[20] J.H. Kim, Y.J. Song, J.S. Rhyee, B.S. Kim, S.D. Park, H.J. Lee, J.W. Shin, Phys Rev B, 87 (2013) 6.
[21] Y.B. Zhai, Q.S. Zhang, J. Jiang, T. Zhang, Y.K. Xiao, S.H. Yang, G.J. Xu, J Mater Chem A, 1 (2013) 8844-8847.
[22] J.B. Vaney, G. Delaizir, E. Alleno, O. Rouleau, A. Piarristeguy, J. Monnier, C. Godart, M. Ribes, R. Escalier, A. Pradel, A.P. Goncalves, E.B. Lopes, G.J. Cuello, P. Ziolkowski, E. Muller, C. Candolfi, A. Dauscher, B. Lenoir, J Mater Chem A, 1 (2013) 8190-8200.
[23] J. Dong, W. Liu, H. Li, X. Su, X. Tang, C. Uher, J Mater Chem A, 1 (2013) 12503-12511.
[24] B. Feng, J. Xie, G. Cao, T. Zhu, X. Zhao, J Mater Chem A, 1 (2013) 13111-13119.
[25] H. Chen, C. Yang, H. Liu, G. Zhang, D. Wan, F. Huang, Crystengcomm, 15 (2013) 6648-6651.
[26] T.H. Zou, X.Y. Qin, D. Li, G.L. Sun, Y.C. Dou, Q.Q. Wang, B.J. Ren, J. Zhang, H.X. Xin, Y.Y. Li, Applied Physics Letters, 104 (2014).
[27] T.H. Zou, X.Y. Qin, D. Li, B.J. Ren, G.L. Sun, Y.C. Dou, Y.Y. Li, L.L. Li, J. Zhang, H.X. Xin, Journal of Applied Physics, 115 (2014) 053710.
[28] T.H. Zou, X.Y. Qin, D. Li, L.L. Li, G.L. Sun, Q.Q. Wang, J. Zhang, H.X. Xin, Y.F. Liu, C.J. Song, Journal of Alloys and Compounds, 588 (2014) 568-572.
[29] J. Yang, H.-L. Yip, A.K.Y. Jen, Adv Energy Mater, 3 (2013) 549-565.
[30] D.G. Zhao, M. Zuo, J.F. Leng, H.R. Geng, Intermetallics, 40 (2013) 71-75.
[31] H. Park, S.J. Lee, S. Kim, H.W. Ryu, S.H. Lee, H.H. Choi, I.W. Cheong, J.H. Kim, Polymer, 54 (2013) 4155-4160.
[32] A. Kosuga, K. Tsuchiya, M. Matsuzawa, J Alloy Compd, 568 (2013) 118-123.
[33] B. Feng, H.P. Martin, A. Michaelis, J Electron Mater, 42 (2013) 2314-2319.
[34] Y. Lu, K. Sagara, Y. Matsuda, L. Hao, Y.R. Jin, H. Yoshida, Ceram Int, 39 (2013) 6689-6694.
[35] Y. Yang, F.Y. Ma, C.H. Lei, Y.Y. Liu, J.Y. Li, J Mech Phys Solids, 61 (2013) 1768-1783.
[36] B. Kuhn, W. Kaefer, K. Fess, K. Friemelt, C. Turner, M. Wendl, E. Bucher, Phys. Status Solidi A-Appl. Res., 162 (1997) 661-671.
[37] J.S. Im, J. Yun, J.G. Kim, Y.S. Lee, Curr Org Chem, 17 (2013) 1424-1433.
[38] J.Q. Li, L.F. Li, S.H. Song, F.S. Liu, W.Q. Ao, J Alloy Compd, 565 (2013) 144-147.
[39] H. Bark, J.S. Kim, H. Kim, J.H. Yim, H. Lee, Curr Appl Phys, 13 (2013) S111-S114.
[40] T. Plirdpring, K. Kurosaki, A. Kosuga, T. Day, S. Firdosy, V. Ravi, G.J. Snyder, A. Harnwunggmoung, T. Sugahara, Y. Ohishi, H. Muta, S. Yamanaka, Adv Mater, 24 (2012) 3622-3626.
[41] L. Xue, B. Xu, D. Zhao, L. Yi, Comp Mater Sci, 90 (2014) 143-147.
[42] D. Zou, S. Xie, Y. Liu, J. Lin, J. Li, J Alloy Compd, 570 (2013) 150-155.
[43] J.L. Cui, Y.P. Li, Z.L. Du, Q.S. Meng, H. Zhou, J Mater Chem A, 1 (2013) 677-683.
[44] V.K. Gudelli, V. Kanchana, G. Vaitheeswaran, A. Svane, N.E. Christensen, J Appl Phys, 114 (2013).
[45] J.M. Yang, Y.L. Yan, Y.X. Wang, G. Yang, Rsc Adv, 4 (2014) 28714-28720.
[46] X.Y. Li, D. Li, H.X. Xin, J. Zhang, C.J. Song, X.Y. Qin, Journal of Alloys and Compounds, 561 (2013) 105-108.
[47] J.Y. Cho, Z. Ye, M.M. Tessema, R.A. Waldo, J.R. Salvador, J. Yang, W. Cai, H. Wang, Acta Mater, 60 (2012) 2104-2110.
[48] A. Kosuga, T. Plirdpring, R. Higashine, M. Matsuzawa, K. Kurosaki, S. Yamanaka, Appl. Phys. Lett., 100 (2012) 042108.
[49] Y.P. Li, Q.S. Meng, Y. Deng, H. Zhou, Y.L. Gao, Y.Y. Li, J.F. Yang, J.L. Cui, Appl Phys Lett, 100 (2012).
[50] C. Rincon, S.M. Wasim, G. Marin, Appl Phys Lett, 80 (2002) 998-1000.
[51] Y. Zhang, J.H. Bahk, J. Lee, C.S. Birkel, M.L. Snedaker, D. Liu, H. Zeng, M. Moskovits, A. Shakouri, G.D. Stucky, Adv Mater, (2014).
[52] P. Buffat, J.P. Borel, Physical Review A, 13 (1976) 2287-2298.

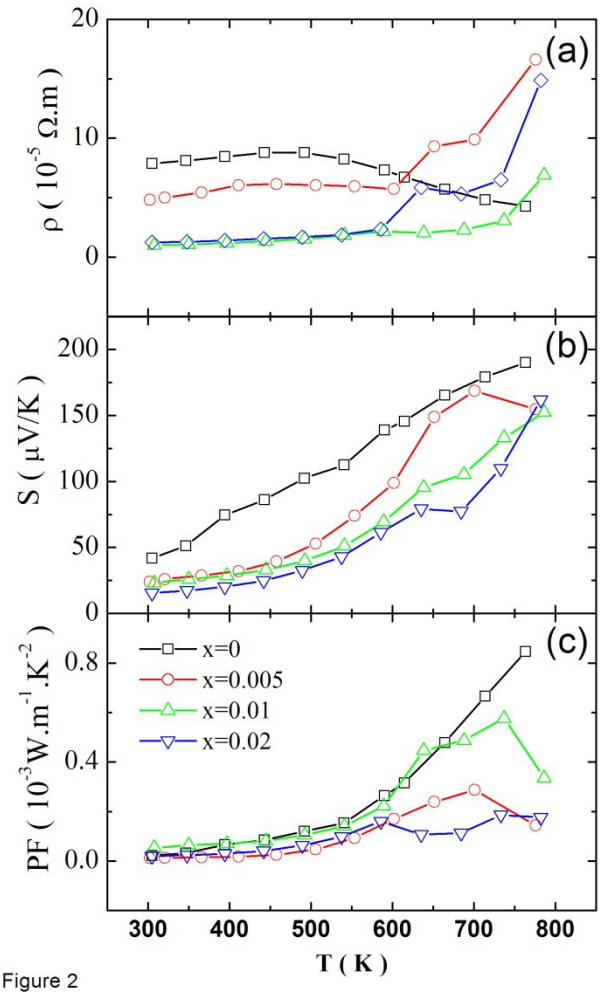

Figure 2

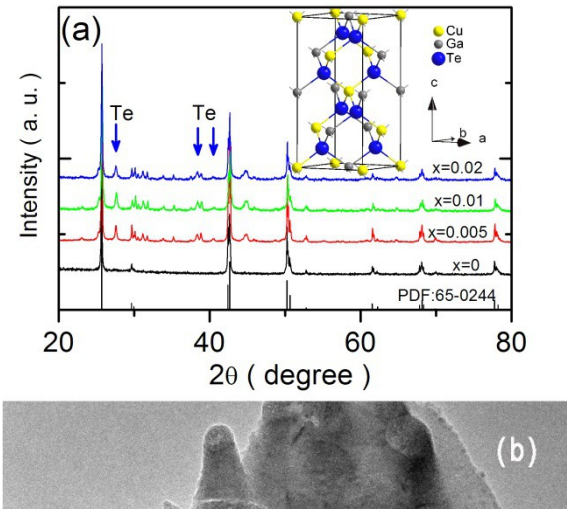

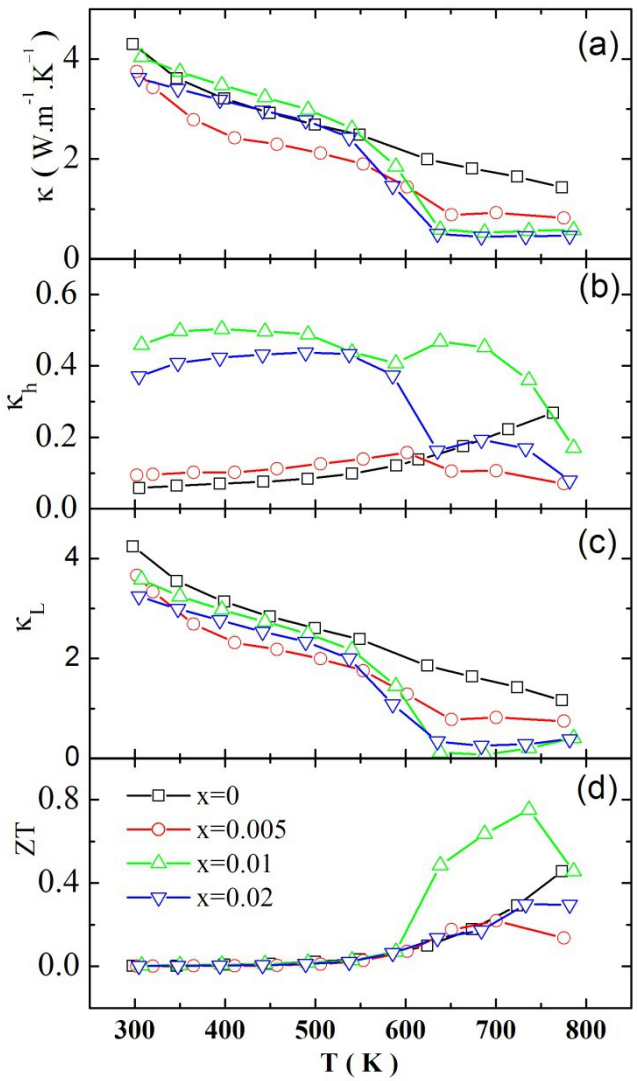

Figure 3